534. 6. 011. 5 : 532

A Study of Pseudo-Shock*

(1st Report, λ-Type Pseudo-Shock)

By Teiichi TAMAKI**, Yukio TOMITA***,
and Ryuichiro YAMANE****

A pseudo-shock occurs, when a supersonic flow is decelerated to subsonic in a duct surrounded by walls. Its shape is influenced by the main stream Mach number and the condition of the boundary layer. In this study, the authors investigated the phenomena of the λ-type pseudo-shocks experimentally, and obtained the distribution of the static and total pressure in the duct in the pseudo-shock region. The results show that the mechanism of the pseudo-shock can be divided into two parts; the first is the upstream region in which the supersonic flow is gradually decelerated to sonic, and in the second downstream region the high speed flow in the central core is mixed with the low speed flow near the walls.

1. Introduction

When a supersonic flow is decelerated to subsonic in a duct surrounded by solid walls, such as a supersonic diffuser and a channel made up of adjacent blades of a supersonic axial compressor, the so-called pseudo-shock is known to occur in place of a single normal shock wave by the effect of the boundary layer on the wall surface.

The static pressure on the wall increases gradually over a rather long distance in contrast with discontinuous pressure rise by the normal shock wave. The flow with the pseudo-shock is so different from that expected from the inviscid theory that the diffusing performance of the duct is deteriorated. So knowledge of the pseudo-shock is important for the designer of the supersonic-subsonic decelerating passage.

The interaction between the shock waves and the boundary layer in the pseudo-shock region is so complex that no theoretical analysis has been published except Crocco's shockless model[1].

On the other hand, experimental results were reported by some investigators. Lukasiewicz[2] observed the pseudo-shock in a square duct with Schlieren method. Neumann and Lustwerk[3] measured wall static pressures in the pseudo-shock region in circular ducts. They concluded that the wall static pressure increased monotonously, that the length of the pseudo-shock defined as the distance from the position of the first pressure rise to that of the maximum pressure was 8 ~ 13 times the duct diameter, and that the overall pressure rise was nearly equal to that of a normal shock wave for the same Mach number. Using a divergent duct, Bogdonoff[4] indicated that the wall static pressure increased monotonously and the separation occurred at the Mach number about 1.35. In these experiments, they treated the phenomena of the pseudo-shocks only with the wall static pressure. The mechanism of the pseudo-shock still remains unclear theoretically and experimentally.

In this paper, the authors try to clarify experimentally the mechanism of the whole region of the pseudo-shock and to give useful basis for theoretical analysis. For this purpose the static and total pressured were measured and Schlieren photographs were taken for the pseudo-shock in a slightly divergent duct.

It is inferred from the previous researches and authors' preliminary experiment that the mechanism of the pseudo-shock is as follows. Although the wall pressure rises over about 10 times the duct diameter, the Schlieren pictures show that a series of shock waves characterising the pseudo-shock, appears only in the upstream region, and in the downstream region where no shock appears, the static pressure continues to increase. Therefore it seems that the supersonic main flow is once decelerated to sonic by the series of shock waves and

* Received 24th September, 1968.
** Graduate Student, Tokyo Institute of Technology, Meguro-ku, Tokyo.
*** Professor, Faculty of Engineering, Tokyo Institute of Technology.
**** Research Associate, Faculty of Engineering, Tokyo Institute of Technology.

then turns into a steady subsonic flow mixing with a low speed layer near the wall. The wall pressure rises continuously in the mixing process. Hence the pseudo-shock region is divided into two regions; an upstream region with a series of shock waves (named shock region) and a downstream subsonic mixing region.

The purpose of this report is to make clear the features of these two regions and of the low speed layer near the wall which controls the flow throughout two regions.

According to the Schlieren observation, pseudo-shocks can be classified into two types for different Mach numbers and Reynolds numbers. In the first type (named λ-type), the leading shock wave is nearly normal at the duct center, bifurcating near the walls. In the second (named X-type), it is X-shaped without normal stem at the duct center. For the λ-type pseudo-shock the total pressure change of the flow through the normal part may be different from that through the bifurcated part near the wall. As a comparatively low Mach number supersonic flow ($M<2.0$) is more often encountered in the ordinary mechanical engineering, the authors deal with the λ-type pseudo-shock which occurs under such conditions as the first step.

2. Nomenclature

A, A_a : crosssectional area and wetted area of the duct
c : area ratio ($\equiv A_2/A_1$)
c_f : local skin friction coefficient
c_p : specific heat at constant pressure
D : $\equiv 1+1\Big/\dfrac{\gamma-1}{2}M_\infty^2$
F : nondimensional skin friction force
H : ratio of displacement thickness to momentum thickness
h, h' : half height and width of the duct
M : Mach number
P, P_0 : static and total pressure respectively
R_e : Reynolds number characterized by the distance
T : temperature
U : velocity
V : velocity ratio ($\equiv U_2/U_1$)
x, X : distance measured along the flow direction from the plate leading edge and from the first shock position respectively
y : height from the wall
γ : ratio of specific heats
δ, δ^*, θ : boundary layer thickness, displacement thickness and momentum thickness respectively
ρ : density
τ : shear stress at the wall

Subscripts

∞, w : condition in the main stream and at the wall
S, T, x : condition in the settling chamber, at the throat and at the distance x respectively
1, 2, m : condition at the starting position and the end position of the pseudo-shock and mean value respectively

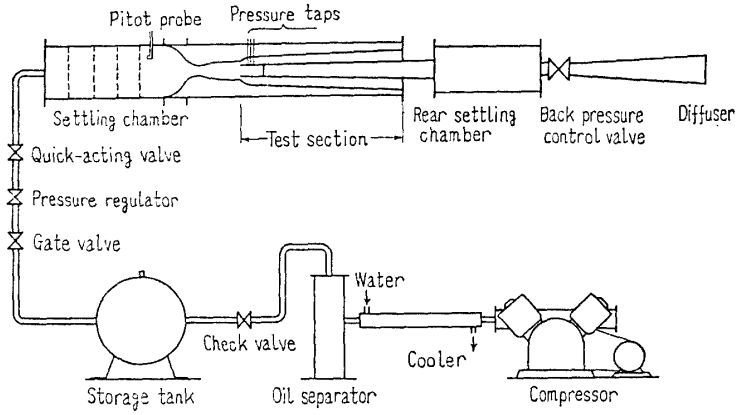

Fig. 1 Schematic experiment

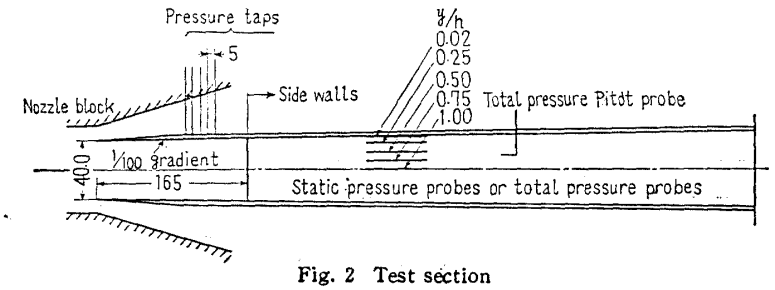

Fig. 2 Test section

3. Experimental equipment and methods of measurement

3·1 Experimental equipment

A blowdown tunnel and other experimental equipment are shown schematically in Fig. 1. According to the previous experiments, pseudo-shocks were obsereved when Mach number was as low as 1.6, which shows that such low Mach number is enough for investigating the mechanism of the pseudo-shock. For this reason, the nozzle outlet Mach number 1.4 was selected to have the Mach number 1.4 ~ 1.8 in the test section. As shown in Fig. 2, the test section consists of a rectangular duct surrounded by two flat plates and side walls. Top and bottom plates cut

off the boundary layers on the nozzle walls, and make new boundary layers upstream of the pseudo-shock. The side plates set from 165 mm downstream of the leading edge, also cut off the side wall boundary layers and assure a weak effect of the side plate boundary layers on the mechanism of the pseudo-shock. Both of the top and bottom plates are sloped 1 mm per 100 mm from the center line, forming a slightly divergent duct so as to make the pseudo-shocks stable. The 1 200 mm long test section is 40 mm in height and 50 mm in width at the leading edge and is 30 mm in width after the side plates.

3·2 Methods of measurement

(1) Measurement of the upstream total pressure

When the flow is supersonic in the nozzle and the test section, the entropy change is so small that the total pressure in the test section can be replaced by that in the settling chamber. The total pressure in the settling chamber (P_{oS}) was measured with an L-shaped Pitot probe and a Bourdon tube pressure gauge. It was confirmed to be identical with that in the test section by the measurement of the boundary layer.

(2) Measurement of the wall static pressure

The wall static pressure change throughout the pseudo-shock region was measured through the surface holes drilled with the interval of 5 mm on the plate with the mercury manometers. In the subsonic mixing region, the static pressure in the duct can be replaced by the wall static pressure, since it is considered to be constant in the duct section.

(3) Measurement of the static pressure in the duct

In the shock region, the static pressure at the duct center is different from that near the wall, because the rapid change of the static pressure at the duct center is reduced to a gradual change near the wall. For this reason, it is necessary to measure the static pressure at every position in the duct. The static pressure was measured with the static probes (diameter 1.5 mm) which were set at fixed distances from the wall, y/h=0.02, 0.25, 0.50, 0.75, 1.00, moved continuously in the flow direction. The relation between the pressure and the static probe position was recorded with the pressure heads and the electro-magnetic oscillograph.

(4) Measurement of the total pressure in the duct

The flow in the pseudo-shock region is so different from that of the inviscid normal shock wave theory, that the total pressure is constant neither along nor across the flow. Then it is necessary to measure the total pressure at every position in the duct. In the shock region it was measured with the same method as that for the static pressure except that the static pressure probes were replaced by the total pressure probes. In the subsonic mixing region, it was measured with the Pitot probe (diameter 0.4 mm) traversed across the duct.

(5) Schlieren observation

For the visual observation of the pseudo-shock, the Schlieren photographs were taken for each run.

3·3 Experimental method

After the opening of the back pressure control valve was so adjusted that the pseudo-shock occurred at the prescribed position, the compressed air in the storage tank was released to the nozzle and the test section through the pressure regulator, the quick-acting valve and the settling chamber. The flow being steady, the static pressure, total pressure etc. were measured and the Schlieren photograph was taken.

3·4 Flow in test section without pseudo-shock (Mach number and boundary layer)

The pseudo-shock phenomenon seems to be affected by the incoming Mach number and the upstream boundary layer. For this reason, the boundary layer and the Mach number in the test section without the pseudo-shock were investigated as the preliminary test. Figure 3 shows the distribution of the wall pressure and the main flow Mach number obtained from the wall pressure P_w and the settling chamber total pressure P_{oS}. The broken lines correspond to the inviscid one-dimensional flow and the solid lines to the flow modified with the approximate boundary layer calculation.

For the former the main stream Mach number and the wall static pressure can be calculated from the following equations

$$\left(\frac{A}{A_T}\right)^2=\frac{1}{M_\infty^2}\left[\frac{2}{\gamma+1}\left(1+\frac{\gamma-1}{2}M_\infty^2\right)\right]^{(\gamma+1)/(\gamma-1)} \quad \cdots\cdots(1)$$

$$\frac{P_{oS}}{P_w}=\left(1+\frac{\gamma-1}{2}M_\infty^2\right)^{\gamma/(\gamma-1)} \quad \cdots\cdots(2)$$

For the latter the method of calculation is as

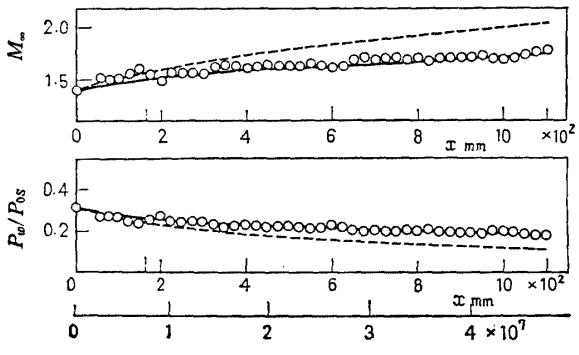

Fig. 3 Distribution of Mach number and wall static pressure

follows; assuming the main flow to be isentropic, the integral momentum equation for the turbulent boundary layer is written[5]

$$\frac{c_f}{2}=\frac{d\theta}{dx}+\left[\frac{2-M_\infty^2+H}{M_\infty\left(1+\frac{\gamma-1}{2}M_\infty^2\right)}\frac{dM_\infty}{dx}\right]\theta \quad \cdots(3)$$

When the Mach number change is small along the stream, the increase of the momentum thickness $\Delta\theta$ in the small range $[x,\ x+\Delta x]$ is approximately described

$$\Delta\theta=\left(\frac{c_f'}{2}\right)_x\Delta x-\left[\frac{2-M_\infty^2+H}{M_\infty\left(1+\frac{\gamma-1}{2}M_\infty^2\right)}\theta\right]_x\Delta M_\infty' \quad \cdots(4)$$

where c_f' is the local friction coefficient and $\Delta M_\infty'$ is the Mach number change in the range $[x-\Delta x,\ x]$. Assuming a constant stagnation enthalpy and the 1/7 power law velocity profile in the boundary layer, the form parameter H can be calculated using the equations

$$\frac{\delta^*}{\delta}=1-7(D-1)\left\{\frac{D^3}{2}\ln\frac{D}{D-1}-\frac{D^2}{2}-\frac{D}{4}-\frac{1}{6}\right\} \quad \cdots(5)$$

$$\frac{\theta}{\delta}=1-\frac{\delta^*}{\delta}-7(D-1)\left\{\frac{D^{7/2}}{2}\ln\frac{\sqrt{D}+1}{\sqrt{D}-1}-D^3-\frac{D^2}{3}-\frac{D}{5}-\frac{1}{7}\right\} \quad \cdots(6)$$

where $D\equiv1+1\Big/\frac{\gamma-1}{2}M_\infty^2$. According to Tucker[6], c_f' is given for no pressure gradient

$$c_f'=0.026\,2R_{e\infty}^{-1/7}\left(\frac{2}{2+\frac{\gamma-1}{2}M_\infty^2}\right)^{5/7} \quad \cdots(7)$$

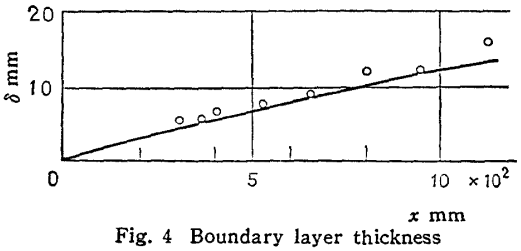

Fig. 4 Boundary layer thickness

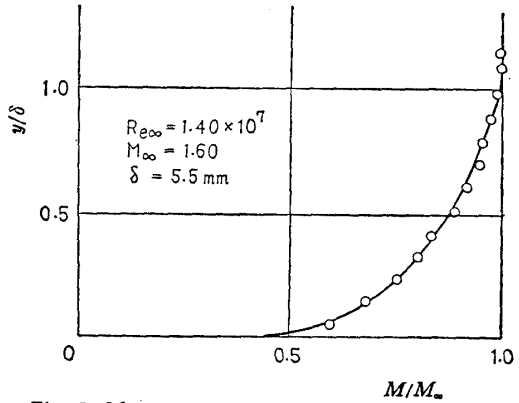

Fig. 5 Mach number profile in boundary layer

The momentum thickness θ and the displacement thickness δ^* can be calculated, substituting Eqs. (5), (6) and (7) into (4), computing $\Delta\theta$ step by step from the leading edge and using Eqs. (5) and (6). The effective area of the duct can be estimated from

$$A=(2h-2\delta^*)(h'-2\delta^{*\prime}) \quad \cdots(8)$$

with the displacement thickness on the plate δ^* and on the side wall $\delta^{*\prime}$. Then the main flow Mach number and the wall static pressure can be calculated using Eqs. (1) and (2).

Figure 3 shows that the calculated results agree well with the experiment in the range $x>200$ mm. Figure 4 shows a comparison of the calculated boundary layer thickness (solid line) with the experimental results.

Figure 5 indicates a typical Mach number profile in the boundary layer ($M_\infty=1.60$, $R_{e\infty}=1.40\times10^7$). The solid line shows the calculated results under the assumption of a constant total enthalpy and the 1/7 power law velocity profile in the boundary layer. This corresponds to the boundary layer just before the pseudo-shock investigated in detail in the following section and the boundary layer thickness was 5.5 mm.

4. Experimental results

4·1 Effect of M_∞ and $R_{e\infty}$ on shape of pseudo-shock

Figures 6 and 7 show the wall pressure distributions in the pseudo-shock region occurring at various positions. Figure 6 shows the pressure distribution over the whole range of the test section

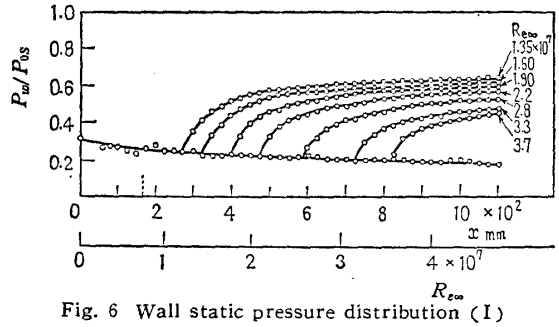

Fig. 6 Wall static pressure distribution (I)

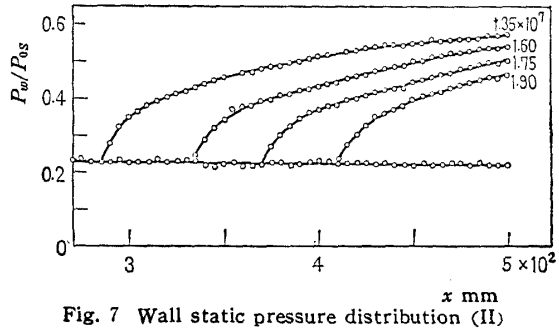

Fig. 7 Wall static pressure distribution (II)

and Fig. 7 the details in the upstream region of pseudo-shock.

The Schlieren photographs of the shock region are shown in Fig. 8. According to these photographs and previous researches, the pseudo-shock seems to be λ-type when the main flow Mach number is $1.4 \sim 1.8$, $R_{e\infty}=1\times10^7 \sim 4\times10^7$ and the ratio of the boundary layer thickness to the half duct height δ/h is in moderate range ($\delta/h \sim 0.1$). Though strengths and lengths of these λ-type pseudo-shocks are different for various M_∞, $R_{e\infty}$ and δ/h, they show similar features as a whole, and the mechanism of the λ-type pseudo-shock is considered to be essentially identical. Therefore a certain combination of M_∞, $R_{e\infty}$ and δ/h can be selected without losing the generality for the investigation of the mechanism of the λ-type pseudo-shock. In this research as the representative case, the flow of a pseudo-shock for $M_\infty=1.62$, $R_{e\infty}=1.60\times10^7$ and $\delta/h=0.2$, was investigated in detail.

4·2 Flow condition in pseudo-shock region

Figure 9 shows the static pressure distribution in the duct, which was measured along the flow direction in the shock region. The ordinate is the nondimensional pressure P/P_{0S} and the abscissa is the distance from the position of the leading shock wave in the main stream. This result is the averaged one neglecting the small fluctuations due to the unsteadiness of the pseudo-shock.

Figure 10 shows the total pressure profile at some duct sections in the subsonic mixing region. The ordinate and the abscissa are the distance from the wall y/h and the nondimensional pressure P_0/P_{0S} respectively. Figure 11 shows the total pressure distribution along the flow for the fixed distances from the wall. The pressure was measured continuously in the shock region and obtained from Fig. 10 in the subsonic mixing region. Figure 12 shows the Mach number profiles in the subsonic region, obtained from the total pressure P_0 and the wall static pressure P_w.

5. Discussion

5·1 General view of pseudo-shock

Before the detailed discussion of the mechanism of the pseudo-shock, the pseudo-shock is treated as a whole, that is, the experimental results on the

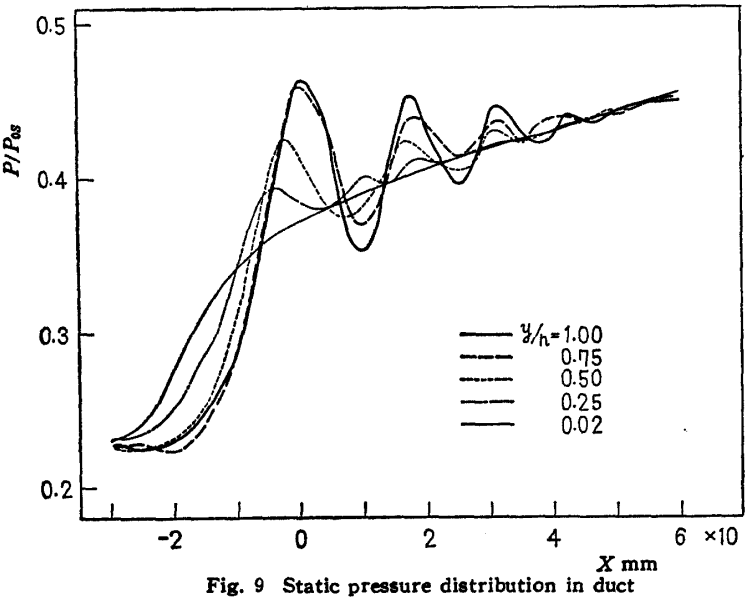

Fig. 9 Static pressure distribution in duct

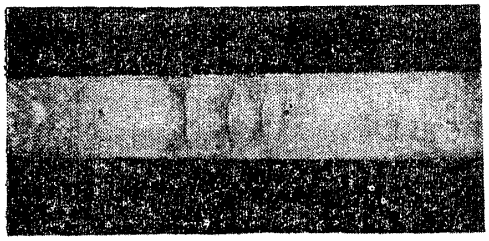

(a) $M_\infty=1.62$, $R_{e\infty}=1.60\times10^7$

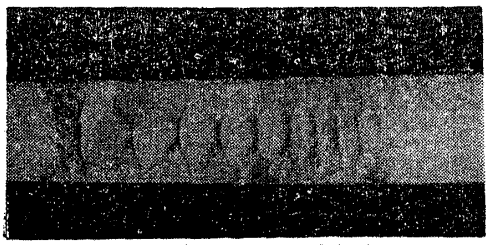

(b) $M_\infty=1.68$, $R_{e\infty}=3.3\times10^7$

Fig. 8 Schlieren photographs

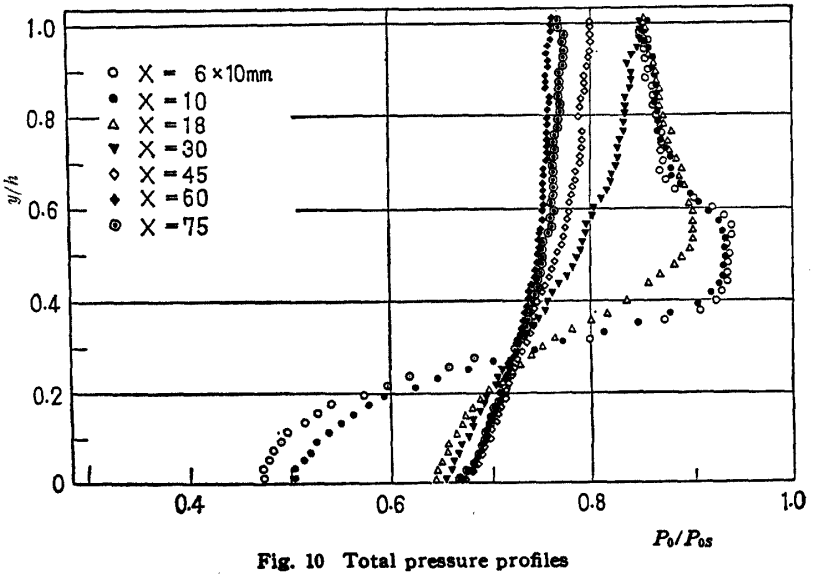

Fig. 10 Total pressure profiles

static pressure rise and on the total pressure loss over the whole region of the pseudo-shock are compared with the calculated results, assuming a one-dimensional flow.

The control surfaces I and II are chosen just before and just after the pseudo-shock respectively. Neglecting the heat transfer at the wall, the following equations hold on the control surfaces

equation of continuity;

$$A_1\rho_1U_1=A_2\rho_2U_2 \quad \cdots\cdots(9)$$

equation of momentum;

$$A_1\rho_1U_1^2-A_2\rho_2U_2^2=\int_{\mathrm{I}}^{\mathrm{II}}AdP+\int_{\mathrm{I}}^{\mathrm{II}}\tau dA_a \quad \cdots\cdots(10)$$

equation of energy;

$$c_pT_1+\frac{1}{2}U_1^2=c_pT_2+\frac{1}{2}U_2^2 \quad \cdots\cdots(11)$$

The right-hand side of Eq. (10) depends on the mechanism of the pseudo-shock and cannot be determined by only the conditions on I and II. Assuming the wall static pressure distribution in the pseudo-shock region to be in the form

$$\frac{A-A_1}{A_2-A_1}=\left(\frac{P-P_1}{P_2-P_1}\right)^n \quad \cdots\cdots(12)$$

the first term can be determined as follows,

$$\int_{\mathrm{I}}^{\mathrm{II}}AdP=(P_2-P_1)\left(\frac{n}{n+1}A_1+\frac{1}{n+1}A_2\right) \quad \cdots\cdots(13)$$

Using Eqs. (9), (10), (11) and (12), we obtain the ratios of the static pressure, the density and the total pressure between I and II

$$\frac{P_2}{P_1}=\frac{n+1}{n+c}\gamma M_1^2(1-V)+1-F \quad \cdots\cdots(14)$$

$$\frac{\rho_2}{\rho_1}=\frac{1}{cV} \quad \cdots\cdots(15)$$

$$\frac{P_{02}}{P_{01}}=\left(\frac{\rho_2}{\rho_1}\right)^{\gamma/(\gamma-1)}\left(\frac{P_2}{P_1}\right)^{-1/(\gamma-1)} \quad \cdots\cdots(16)$$

where the velocity ratio $V(\equiv U_2/U_1)$ is a smaller solution of the quadratic equation

$$\left(\frac{n+1}{n+c}\gamma c-\frac{\gamma-1}{2}\right)M_1^2V^2-\left(\frac{n+1}{n+c}\gamma M_1^2+1-F\right)cV+\frac{\gamma-1}{2}M_1^2+1=0 \quad \cdots\cdots(17)$$

where the wall friction force F is

$$F=\frac{n+1}{n+c}\int_{\mathrm{I}}^{\mathrm{II}}\frac{\tau}{P_1}\frac{dA_a}{A_1} \quad \cdots\cdots(18)$$

Since the wall shear stress depends on the mechanism of the pseudo-shock (the velocity gradient at the wall), it cannot be determined exactly. But because it is considered that the flow in the upstream region of the pseudo-shock separates from the wall and that the wall shear stress is small enough there, the effect of the wall shear stress may be taken into account only in the subsonic mixing region. Assuming the flow condition to be constant throughout this region, F is approximated

$$F=\frac{\gamma}{2}\frac{n+1}{n+c}c_f M_m^2\frac{A_aP_m}{A_1P_1} \quad \cdots\cdots(19)$$

where M_m and P_m are the mean values of the Mach number and the static pressure respectively and c_f is the friction coefficient.

The experimental results for $M_\infty=1.60$ and $R_{e\infty}=1.62\times10^7$ indicate that the static and total pressure ratios are about

$$\frac{P_2}{P_1}=2.65, \quad \frac{P_{02}}{P_{01}}=0.75 \quad \cdots\cdots(20)$$

and the area ratio is $c=1.20$ and n is approximately 3. Calculated F is 0.217, assuming $M_m=0.8$.

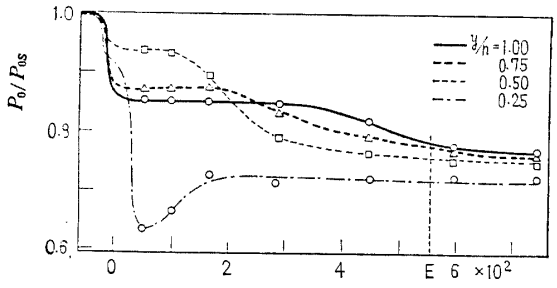

Fig. 11 Total pressure distribution in duct

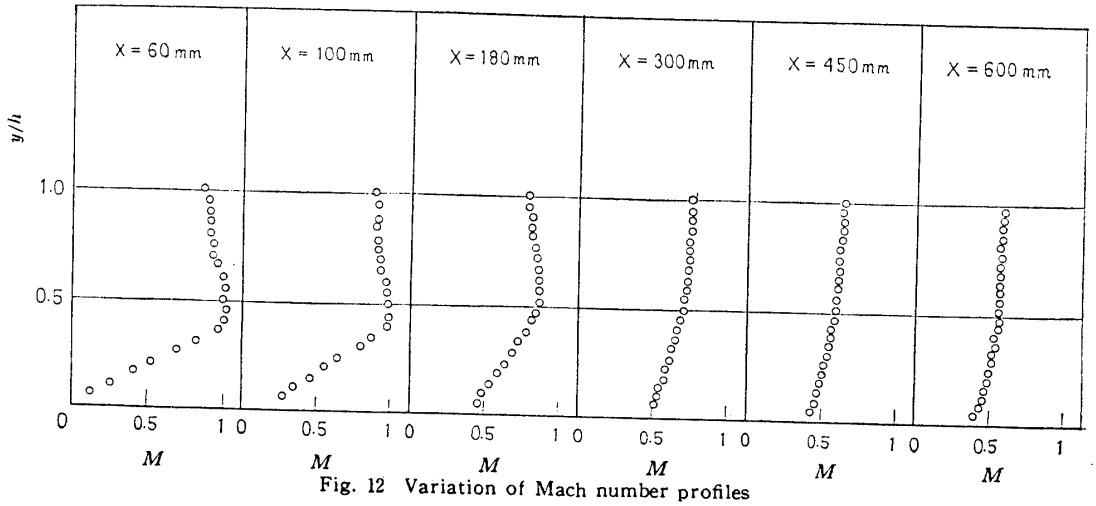

Fig. 12 Variation of Mach number profiles

$c_f=0.003$ and $P_m/P_1=3.16$ which is the value of P_2/P_1 for $F=0$. Substituting these values into Eqs. (14), (15), (16) and (17), we obtain

$$\frac{P_2}{P_1}=2.79,\quad \frac{P_{02}}{P_{01}}=0.798 \qquad \cdots\cdots(21)$$

These results show that the measured static and total pressure ratios are 95% and 94% respectively of the calculated values.

The reasons of this difference are considered to be that in the actual flow, the flows are not uniform on the control surfaces I and II, that there may be the friction force in the upstream region of the pseudo-shock as well, and that the duct wall is not completely adiabatic.

5·2 Wall static pressure distribution

As shown in Figs. 6 and 7, the static pressure does not rise discontinuously even at the foot of the leading shock against the inviscid theory. It increases rapidly but continuously since the rapid pressure rise is diffused out near the wall. The static pressure increases gradually downstream, indicating that the pseudo-shock region is considerably long. But because the test section is a slightly divergent duct, the static pressure increases in the subsonic flow region after the pseudo-shock as well. Therefore the region of the pressure rise due to the pseudo-shock cannot be decided clearly from the wall static pressure distribution.

The pressure rise by the shock wave in the main stream is transmitted upstream through the subsonic part of the boundary layer and the wall static pressure rise starts before the position of the leading shock wave in the main stream. The distance between them is 25 mm and about 4.5δ for the pseudo-shock ($M_\infty=1.62$, $R_{e\infty}=1.60\times10^7$).

5·3 Shock region

In Fig. 8 the Schlieren photograph (b) shows more shock waves and a longer region than (a), because of the higher Mach number and Reynolds number. But in both cases the leading shock waves are λ-type and the shapes of the successive shock waves are similar.

Figure 9 shows that the static pressure in the main flow changes alternately and that its peaks coincide with the shock positions in the Schlieren photograph. The first static pressure rise starts from more upstream position near the wall. It shows that the static pressure begins to rise by the forward leg of the bifurcated leading shock wave.

The static pressure rapidly increases and decreases at the duct center, showing a strong acceleration and deceleration of the flow. In this layer the static pressure ratio by the leading shock wave is $P/P_1=2.1$ which is considerably lower than that by the normal shock wave ($P/P_1=2.9$) for the same Mach number. The reason is that the measured value is somewhat averaged due to the oscillation of the pseudo-shock and to the narrow high pressure region and that the shock wave is not completely normal at the central part. The static pressure rises due to the successive second, third shock waves decrease in this order. It shows that the main flow approaches to sonic and therefore the pressure rise due to the shock waves becomes smaller.

As shown in Fig. 11 the total pressure loss in the shock region is large at $y/h=0.75$, 1.00 and small at $y/h=0.50$. The difference is caused by the facts that for the former the flow passes through a nearly normal shock wave and suffers almost the same loss as through a normal shock wave and for the latter the shock loss is smaller owing to the bifurcated shocks. Most of the total pressure change is caused by the shock waves, especially by the leading shock wave in the main stream. The total pressure of the flow near the wall ($y/h=0.25$) decreases rapidly in the middle of this region, showing that the low speed layer attains the thickness $y/h=0.25$ by the mixing with the main stream.

5·4 Subsonic mixing region

The static pressure rise still continues even after the shock region as shown in Fig. 6. This indicates that the subsonic mixing region plays a considerably important part of the overall pseudo-shock phenomenon. Figures 10 and 12 show that in this region the flow with the complicated velocity profile just after the shock region changes to a more smooth one.

Though the static pressure after the shock region is nearly constant in the duct section, the total pressure is smaller at the duct center as shown in Fig. 10. This may be due to the shock loss difference between the flows through the nearly normal shock and through the bifurcated shock. As shown in Fig. 10, the total pressure profiles change to a more smooth one, owing to the turbulent mixing of the flows in the central core and near the wall. And the static pressure rises according as the velocity profile becomes uniform.

The total pressure distribution in Fig. 11 also shows this mixing process. Near the wall, the mixing occurs in the upstream region and the total pressure rapidly decreases but afterwards increases by the mixing with the main stream. In the main stream, the total pressure also decreases by the mixing, especially at $y/h=0.50$. Figure 11 indicates that the mixing is over near the point E and that the length of the pseudo-shock is about 10 times the duct height.

6. Conclusions

The following results were obtained from the experiment of the λ-type pseudo-shock in a slightly divergent rectangular duct.

(1) The wall static pressure increases gradually over the whole pseudo-shock region. The pressure ratio is considerably smaller than that of the inviscid theory but almost equal to the calculated value considering the effect of the wall friction.

(2) The static pressure in the main stream in the shock region changes alternately along the flow and its peaks coincide with the shock position in the Schlieren photograph.

(3) Just after the shock region, the total pressure is smaller at the duct center. This shows that the shock loss is different between the flows through a nearly normal shock wave and through a bifurcated shock wave, and that it may be the feature of the λ-type pseudo-shock.

(4) Two causes can be considered for the total pressure change; that is, the shock loss and the turbulent mixing. In the duct center the change due to the shock wave is larger than that due to the turbulent mixing and near the wall vice versa. The length of the pseudo-shock is about 10 times the duct height according to the total pressure measurement.

(5) As a result of the above discussion, the mechanism of the pseudo-shock can be considered as follows.

The flow separates from the wall with an adverse pressure gradient and forms a low speed layer near the wall. This layer interacts with the shock waves in the main flow and makes a series of shock waves. The main flow is decelerated by these shock waves to sonic speed. After that, the mixing between the main flow and the low speed layer near the wall changes the complicated velocity profile to a steady smooth one.

Consequently the pseudo-shock can be divided into two major regions: the upstream shock region and the downstream mixing region.

References

(1) L. Crocco: *High Speed Aerodynamics and Jet Propulsion*, Vol. III, Ser. B (1958), p. 110, Princeton.
(2) J. Lukasiewicz: *Jour. Aeron. Sci.*, Vol. 20, No. 9 (1953), p. 617.
(3) E. P. Neumann and F. Lustwerk: *Jour. Appl. Mech.*, Vol. 16, No. 2 (1949), p. 195.
(4) S. M. Bogdonoff: *Princeton Univ. Aeron. Engng. Dept Report*, No. 336 (1955).
(5) S. H. Shapiro: *Compressible Fluid Flow*, Vol. II (1954), p. 1092, Ronald Press.
(6) M. Tucker: *NACA TN* 2337. (1951).